

# Supplementary information for the manuscript “*The effect of clouds and precipitation on the aerosol concentrations and composition in a boreal forest environment*”

Isokääntä et al.

## 1 Data coverage and instrumentation

Table S1 shows the data coverage in % as available hours divided with total hours. Total hours include maximum of 24 data points per day (hourly data), from which points with wind direction 120°-140° and if the trajectory had crossed Kola peninsula were removed before calculating the data coverage. Table S2 shows summary statistics for the measured variables, calculated from the available data.

Table S3 shows the instrumental details for each investigated variable.

**Table S1 Data coverage (in %) for the studied observations between January 2005 and August 2019.**

Variable	Coverage				notes
	DJF	MAM	JJA	SON	
<i>Org, SO<sub>4</sub>, NH<sub>4</sub>, Chl and NO<sub>3</sub></i>	20.0 (37.9)	33.4 (62.8)	40.1/36.0 (74.2/66.6)	28.5 (59.0)	Values in brackets () show the coverage for 2012-19, for JJA the latter value after “/” shows coverage for Chl and NH <sub>4</sub>
<i>T</i>	100.0	100.0	98.7	98.9	
<i>WS</i>	100.0	100.0	99.7	98.0	
<i>NO<sub>x</sub></i>	96.7	97.7	94.8	98.0	
<i>CO</i>	88.4	97.1	94.8	98.1	
<i>SO<sub>2</sub></i>	98.1	94.0	95.8	97.1	
<i>RH</i>	72.8	80.7	81.2	80.9	
<i>SolR</i>	97.4	99.9	99.4	100.0	
<i>WD</i>	100.0	100.0	100.0	100.0	
<i>p</i>	100.0	99.7	100.0	100.0	
<i>eBC</i>	64.8	79.1	66.4	72.9	Measurements start at January 2006
<i>rain<sub>local</sub></i>	94.0	93.2	93.4	99.6	

**Table S2 Median and lower and upper quartiles (Q1 and Q3, respectively) for the measured variables for each season after removing data rows with wind direction between 120°-140° and data rows where trajectory crosses Kola peninsula. Data corresponds to Table S1.**

**Variable Statistics for each season. Med. = Median.**

	DJF			MAM			JJA			SON		
	Q1	Med.	Q3	Q1	Med.	Q3	Q1	Med.	Q3	Q1	Med.	Q3
<i>Org</i> ( $\mu\text{g m}^{-3}$ )	0.45	0.88	1.64	0.64	1.27	2.41	1.32	2.21	3.68	0.56	1.03	1.86
<i>NH<sub>4</sub></i> ( $\mu\text{g m}^{-3}$ )	0.05	0.18	0.36	0.04	0.15	0.29	0.04	0.15	0.30	0.03	0.14	0.30
<i>SO<sub>4</sub></i> ( $\mu\text{g m}^{-3}$ )	0.21	0.52	1.07	0.20	0.37	0.29	0.23	0.39	0.68	0.13	0.33	0.78
<i>Chl</i> ( $\mu\text{g m}^{-3}$ )	0.00	0.01	0.03	0.00	0.01	0.02	0.00	0.01	0.02	0.00	0.01	0.02
<i>NO<sub>3</sub></i> ( $\mu\text{g m}^{-3}$ )	0.06	0.14	0.35	0.05	0.11	0.22	0.07	0.12	0.20	0.05	0.10	0.19
<i>T</i> ( $^{\circ}\text{C}$ )	-7.60	-3.18	-0.27	-0.37	3.26	8.63	12.20	14.94	18.15	1.25	5.17	9.34
<i>WS</i> ( $\text{m s}^{-1}$ )	1.41	1.94	2.62	1.41	1.90	2.57	1.23	1.69	2.27	1.29	1.85	2.58
<i>NO<sub>x</sub></i> ( <i>ppb</i> )	0.72	1.41	2.54	0.28	0.59	1.21	0.19	0.35	0.67	0.40	0.80	1.50
<i>CO</i> ( <i>ppb</i> )	150.44	168.75	204.92	143.74	157.51	171.90	106.94	121.02	136.61	120.98	137.26	155.96
<i>SO<sub>2</sub></i> ( <i>ppb</i> )	0.02	0.10	0.37	0.02	0.08	0.21	0.01	0.04	0.10	0.01	0.03	0.10
<i>RH</i> (%)	92.33	96.23	98.48	50.68	72.05	91.50	55.13	72.67	89.11	85.19	93.74	97.80
<i>SolR</i> ( $\text{W m}^{-2}$ )	-0.11	0.60	6.94	0.49	40.64	239.02	3.70	103.72	333.19	-0.03	1.35	37.91
<i>WD</i> ( $^{\circ}$ )	149.09	200.49	255.73	157.21	217.97	272.50	157.87	212.23	263.30	160.68	206.98	253.40
<i>p</i> ( <i>hPa</i> )	977.38	988.05	997.76	984.07	991.15	998.07	986.36	991.47	996.41	982.17	990.95	999.57
<i>eBC</i> ( $\mu\text{g m}^{-3}$ )	0.13	0.26	0.53	0.09	0.17	0.33	0.08	0.15	0.26	0.10	0.19	0.36
<i>rain<sub>local</sub></i> ( $\text{mm h}^{-1}$ )	0.00	0.00	0.03	0.00	0.00	0.00	0.00	0.00	0.00	0.00	0.00	0.00

**Table S3 List of the measured variables and the measurement devices.**

Variable	Measuring instrument/method
<i>Org, SO<sub>4</sub>, NH<sub>4</sub>, Chl and NO<sub>3</sub></i> ( $\mu\text{g m}^{-3}$ )	ACSM
<i>T</i> ( $^{\circ}\text{C}$ )	Ventilated and shielded sensor (Pt-100)
<i>WS</i> ( $\text{m s}^{-1}$ )	Thies Ultrasonic Anemometer 2D
<i>NO<sub>x</sub></i> ( <i>ppb</i> )	TEI 42 CTL chemiluminescence analyzer
<i>CO</i> ( <i>ppb</i> )	Horiba APMA 370 infrared light absorption analyzer
<i>RH</i> (%)	Calculated from dewpoint until 5/2012, Rotronic MP102H RH sensor since 6/2012
<i>SolR</i> ( $\text{W m}^{-2}$ )	Reemann TP 3 pyranometer, Middleton solar SK08 pyranometer, $\lambda=0.3\text{-}4.8 \mu\text{m}$ , (at height of 18m/35m)
<i>WD</i> ( $^{\circ}$ )	Thies Ultrasonic Anemometer 2D, used value is average of above canopy records
<i>p</i> ( <i>hPa</i> )	Druck DPI 260 barometer, at ground level (180 m a.s.l.)
<i>eBC</i> ( $\mu\text{g m}^{-3}$ )	Magee Scientific Aethalometer with PM10 inlet (models AE-31 and AE-33, AE-31 data corrected by the algorithm suggested by Virkkula et al., 2007), measured at ground level, mass concentration estimated with $\lambda=880\text{nm}$
<i>rain<sub>local</sub></i> ( $\text{mm h}^{-1}$ )	Vaisala FD12P weather sensor at 18 m height

## 2 Supporting figures

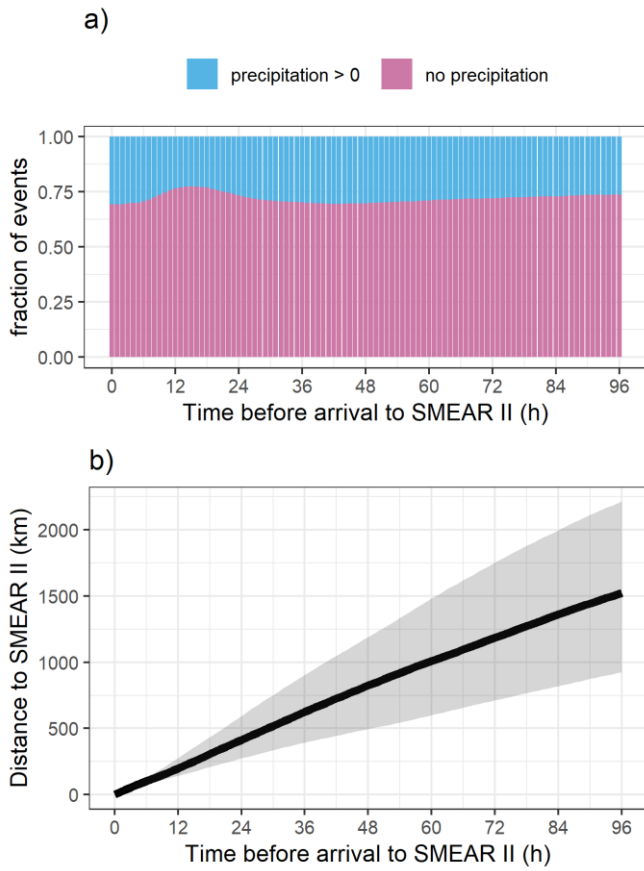


**Figure S1** Fraction of precipitation events (based on ERA-Interim meteorology) along the trajectory is shown in a) and b) shows the median distance from SMEAR II with shaded area showing the 25<sup>th</sup>- 75<sup>th</sup> percentiles.

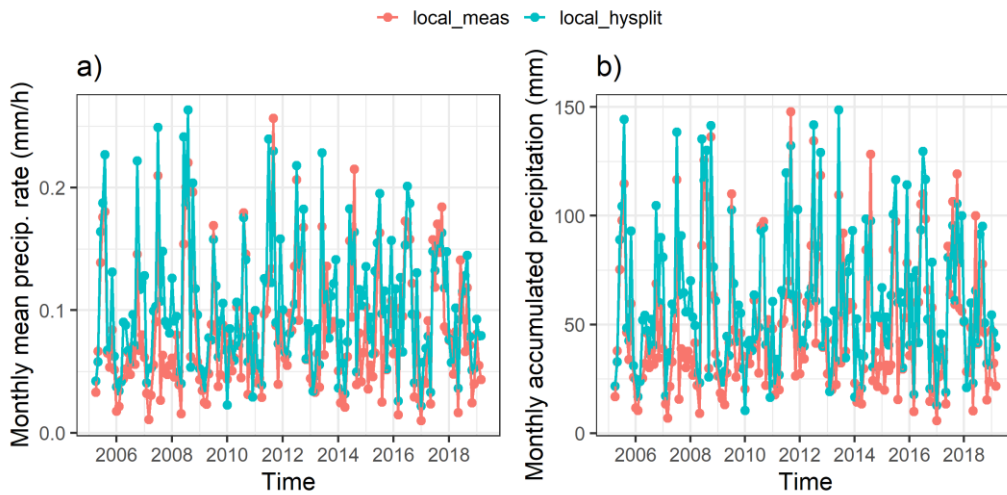


**Figure S2** Precipitation time series of locally measured (red) and HYSPLIT estimate based on ERA-Interim meteorology (blue) as a) monthly mean precipitation rate (mm/h) and b) monthly accumulated precipitation (mm) for SMEAR II. Spearman correlation coefficient between the two in a) is 0.87 and in b) 0.88.

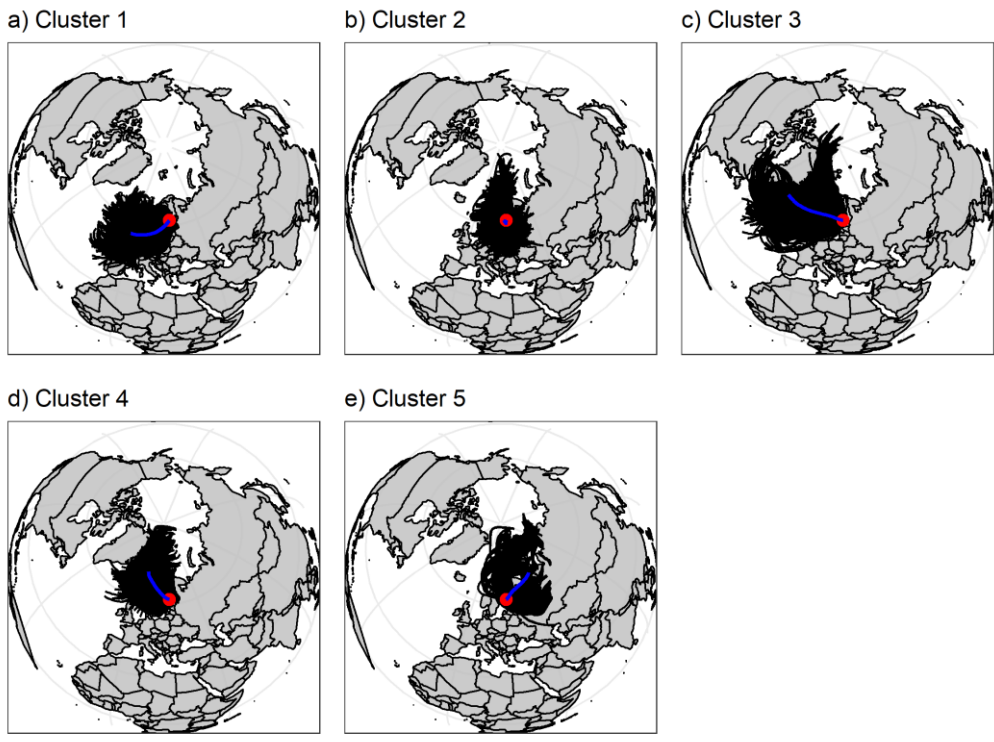


**Figure S3 Geographical air mass source areas determined with the kmeans-clustering for the warm months. The red dot shows the location of SMEAR II and blue line is the cluster centre.**

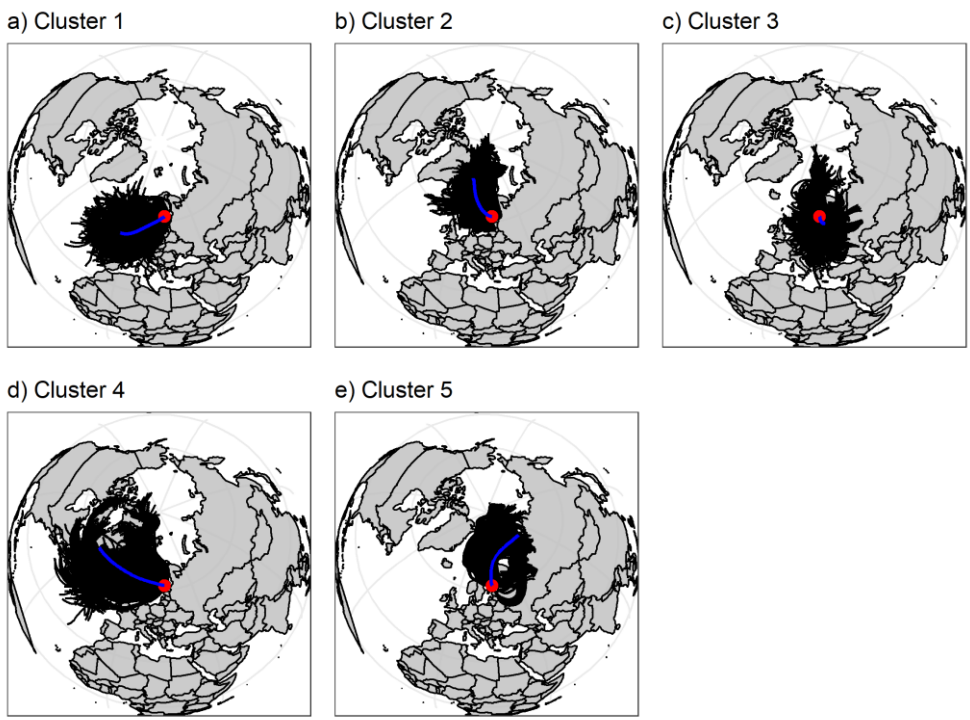


**Figure S4 Geographical air mass source areas determined with the kmeans-clustering for the cold months. The red dot shows the location of SMEAR II and blue line is the cluster centre.**

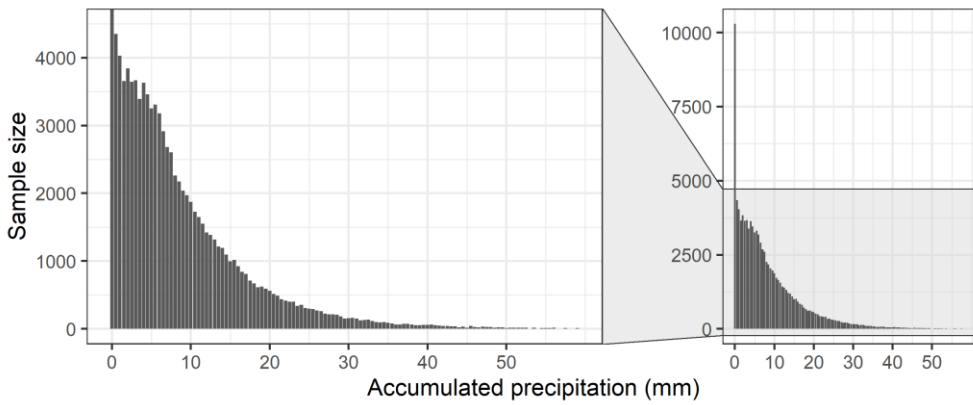


**Figure S5** Sample size in each 0.5 mm bin of accumulated precipitation along the trajectory. Data based on DMPS observations corresponding to Fig. 1 in the main text.

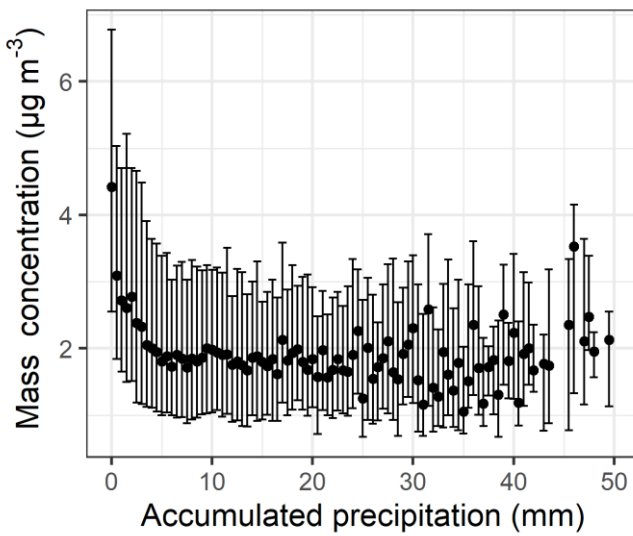


**Figure S6** Particle mass (total sum of the constituents including Org, SO<sub>4</sub>, NO<sub>3</sub>, NH<sub>4</sub>, Chl) evolution derived from the ACSM as a function of accumulated precipitation along the air mass trajectories. The black dots show the median values and bars highlight the 25<sup>th</sup>-75<sup>th</sup> percentiles for each 0.5 mm bin (with 10 or more data points) of accumulated precipitation.

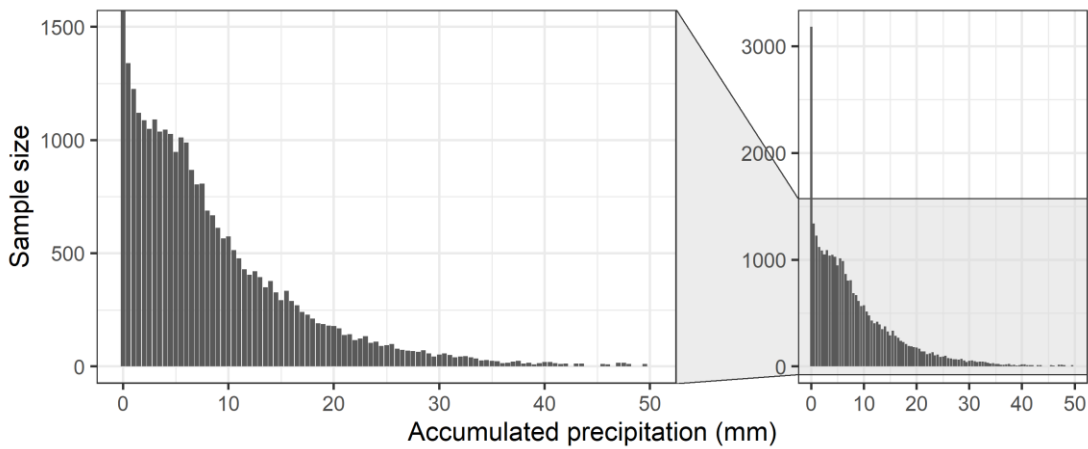


**Figure S7** Sample size in each 0.5 mm bin of accumulated precipitation along the trajectory. Data based on ACSM and Aethalometer derived mass, corresponding to Figure S6

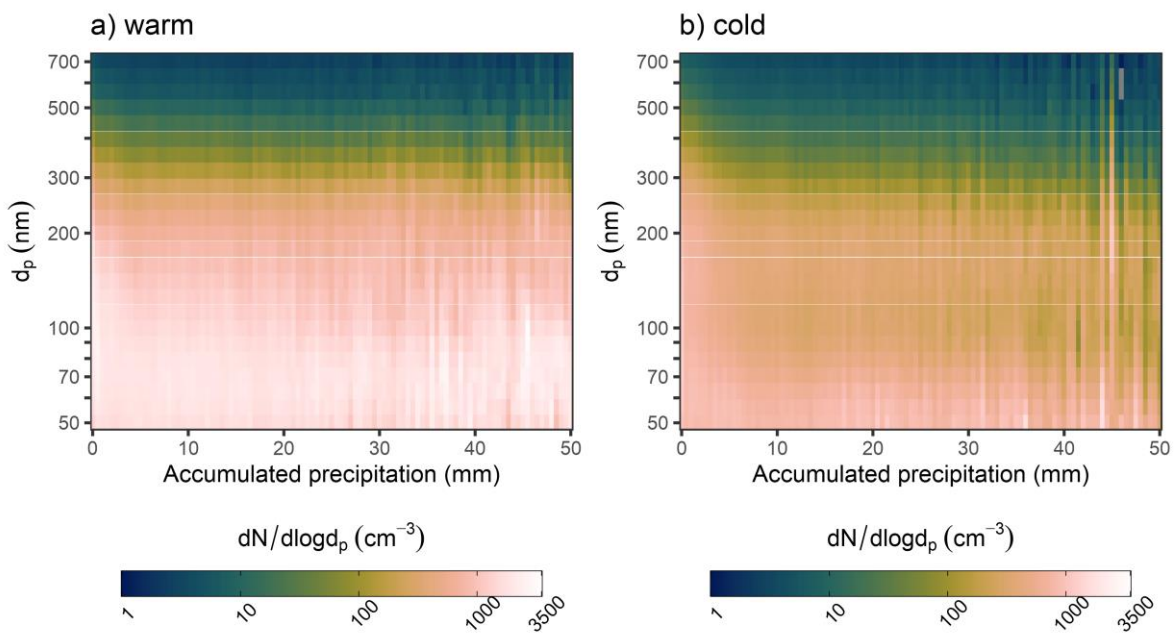


**Figure S8** The aerosol size distribution evolution as a function of the 0-50 mm accumulated precipitation along the 96-hour airmass trajectories for a) warm and b) colder months for  $d_p = 50-700$  nm (representing roughly the size range ACSM measures). Data is shown as medians for binned accumulated precipitation with bin size of 0.5 mm. Grey areas show missing data and/or values where  $dN/d\log d_p < 1$ . The figure includes DMPS data between period of 2012-2019, which overlaps with the composition measurements.

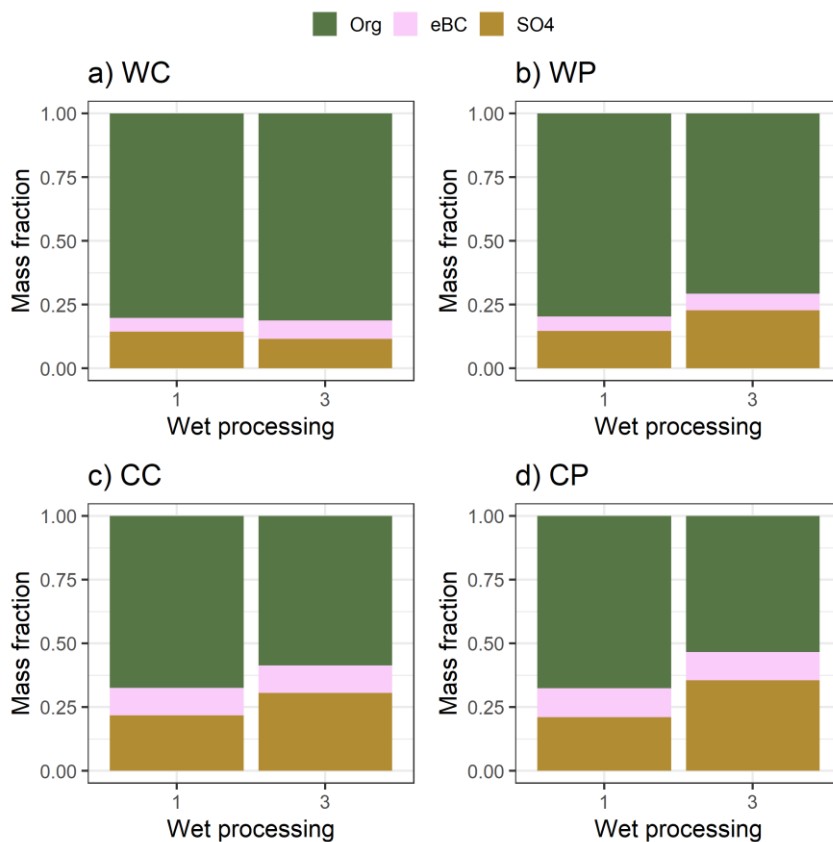


**Figure S9** Chemical composition of the particles for each airmass history groups 1 and 3 as described in Table 2 (main text). Subplots show the airmass sectors (clean and polluted) with the seasonal (warm and cold) division following: a) warm and

clean, b) warm and polluted, c) cold and clean and b) cold and polluted. The figure includes simultaneous observations of these three species, spanning between March 2012 and August 2019.

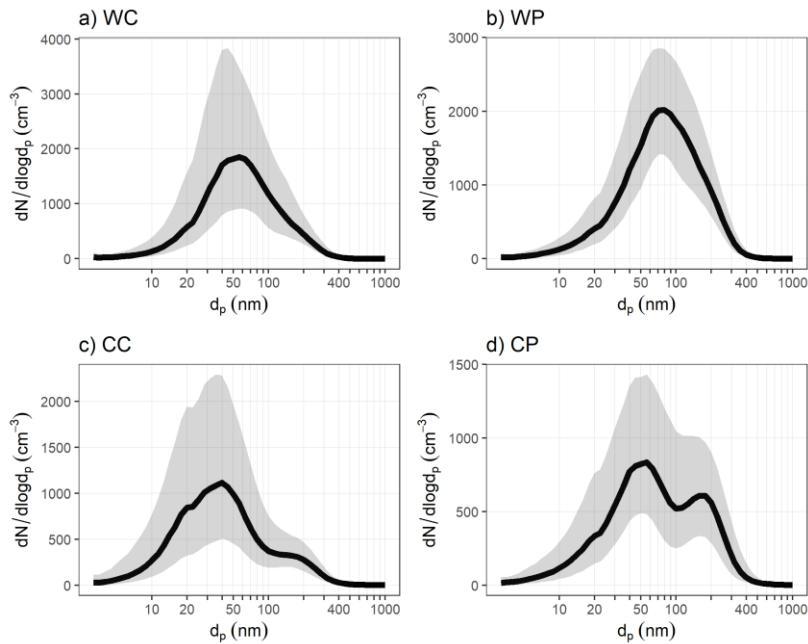


Figure S10 Median size distributions derived from DMPS for the period of 2012-2019, which overlaps with the composition measurements. Subplots show the airmass sectors (clean and polluted) with the seasonal (warm and cold) division followingly: a) warm and clean, b) warm and polluted, c) cold and clean and b) cold and polluted. Please note that only particles larger than  $d_p = 50$  nm are observed with the ACSM measuring the composition.

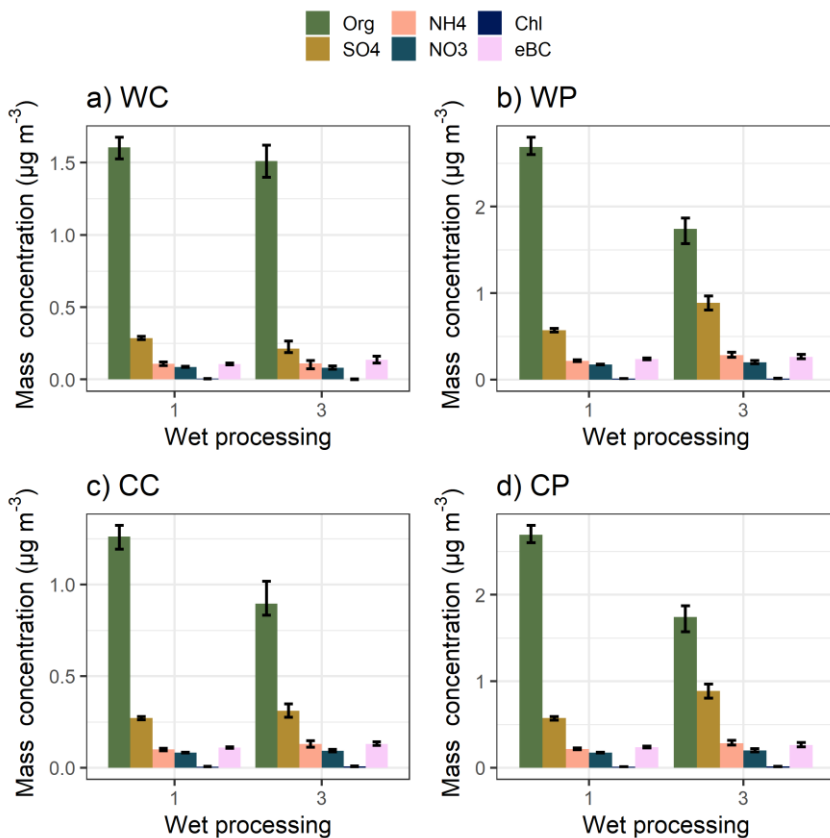


Figure S11 Median particle mass concentration for airmass history groups 1 and 3 as described in Table 2 (main text). Subplots show the airmass sectors (clean and polluted) with the seasonal (warm and cold) division followingly: a) warm and clean, b)

warm and polluted, c) cold and clean and b) cold and polluted. The figure is based on simultaneous observations of these species between March 2012 and August 2019. The whiskers show the 99 % confidence intervals from 1000 bootstrap replicates.

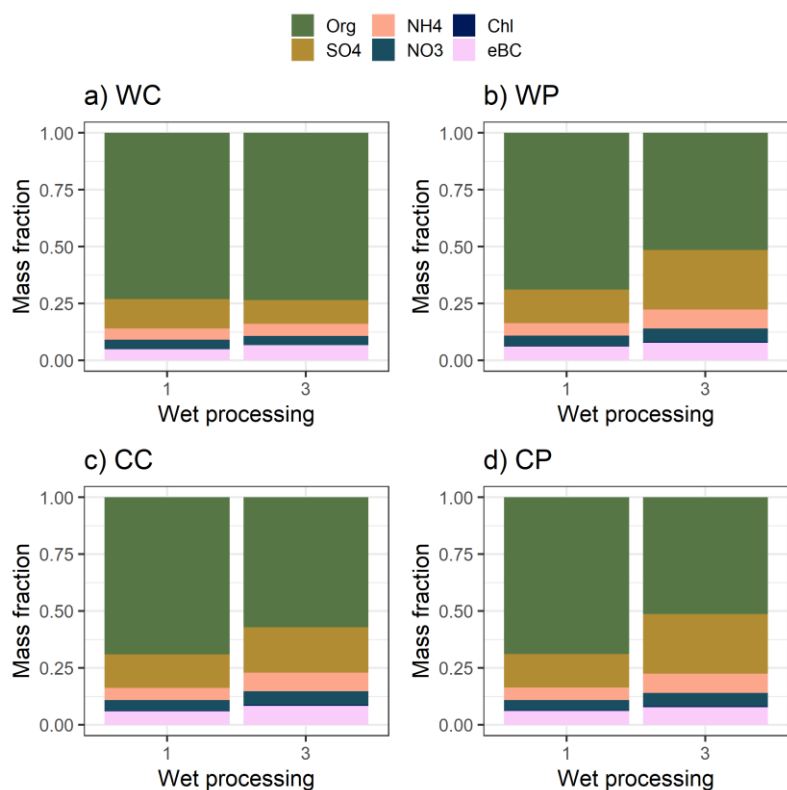


Figure S12 Chemical composition of the particles for each air mass history groups 1 and 3 as described in Table 2 (main text). Subplots show the air mass sectors (clean and polluted) with the seasonal (warm and cold) division following: a) warm and clean, b) warm and polluted, c) cold and clean and b) cold and polluted. The figure includes simultaneous observations of these species, spanning between March 2012 and August 2019.

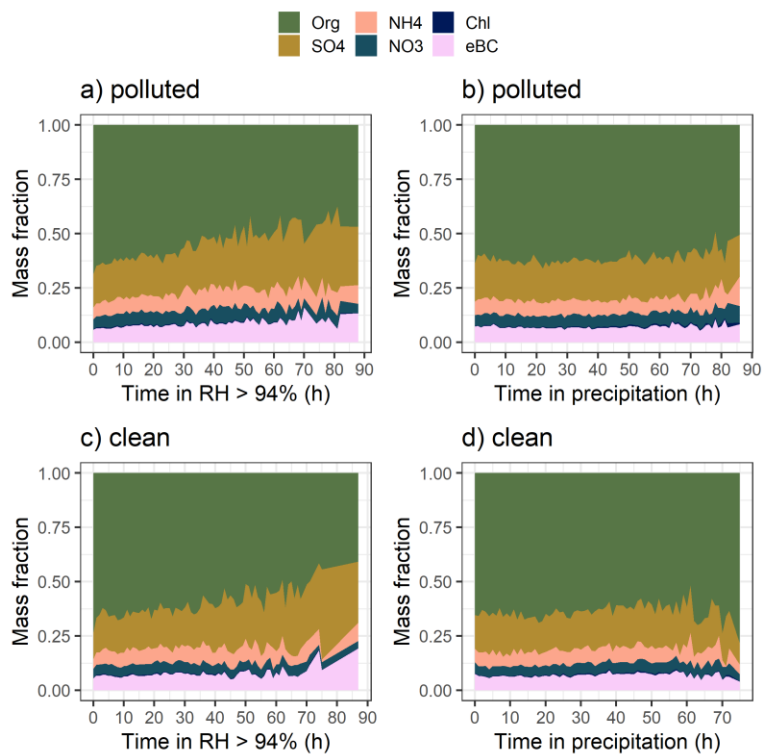




Figure S13 The mass fractions of Org, NH<sub>4</sub>, Chl, SO<sub>4</sub>, NO<sub>3</sub> and eBC for clean and more polluted airmasses (calculated from median values if 10 or more data points were available in the bin) as a function of time spent in high humidity (RH > 94%) conditions (a and c) and in precipitation (b and d) with bin size being one hour for both cases. The figure is based on observations between March 2012 and August 2019.

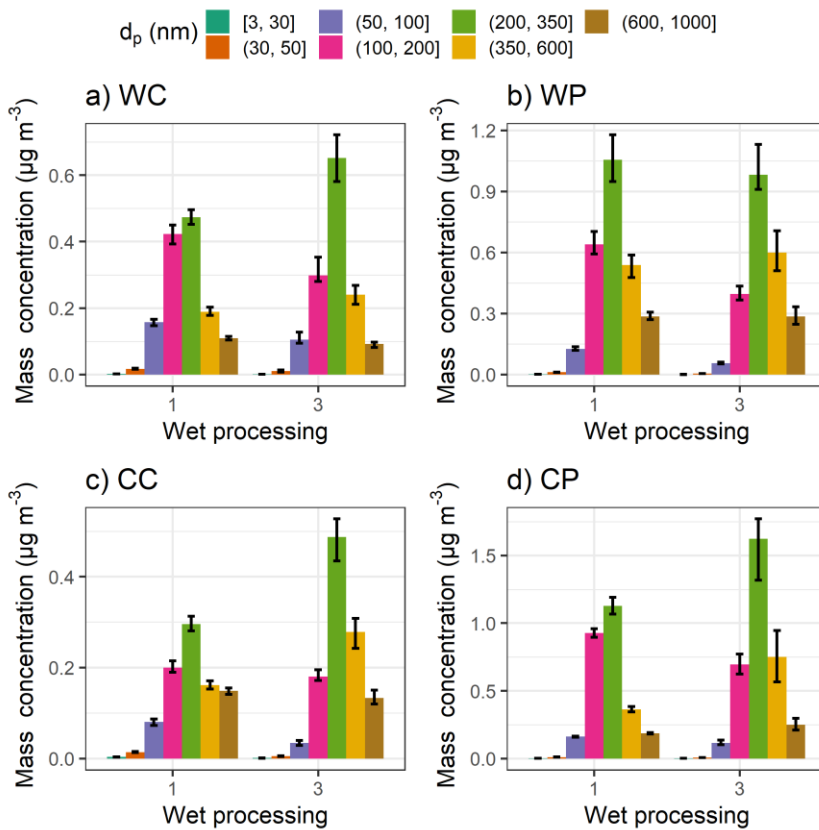


Figure S14 Median particle mass concentration for size bins derived from the DMPS measurements for airmass history groups 1 and 3 as described in Table 2 in the main text. Subplots show the airmass sectors (clean and polluted) with the seasonal (warm and cold) division followingly: a) warm and clean, b) warm and polluted, c) cold and clean and b) cold and polluted. The figure includes simultaneous observations from the DMPS and Org, BC and SO<sub>4</sub> from the ACSM, thus spanning between March 2012 and August 2019. The whiskers show the 99 % confidence intervals from 1000 bootstrap replicates.

### 3 Results from statistical mixed effects models

Table S4-Table S6 show the relative changes in BIC for the fitted mixed effects models and Table S7-Table S9 show the obtained regression coefficients for the full models. Separate models were fitted for each species (Org, eBC and SO<sub>4</sub>) and temperature regimes ( $T_m > 10$  °C and  $T_m < 10$  °C) and the variable groups referred in the tables were presented in Table 1 in the main text. As group 4 (wet processing along trajectory) and its subgroups 4a and 4b are based on the processes along the air mass trajectories, their effects on the model can be considered highly collinear. On the other words, groups 4 and 5 (long-range transport) likely share some part of the model predictive potential.

Relative difference (Table S4-Table S6) close to zero indicates the variable group does not improve the overall fit much, though it does not necessary mean that the variable would not be important in the model considering other properties. The correlation coefficient describes how well the changes in the observed data are captured by the model, larger coefficient indicating from better fit. Each variable group was removed from the full model (marked as “none” in Table S4-Table S6) separately at a time, thus the change in BIC expresses how much each variable group contributes to the model in relative to all other used variable groups. Calculation of BIC is based on the log-likelihood function (Schwarz, 1978; Stoica and Selen, 2004) and is thus sensitive to changes in the data. It is commonly used to compare nested model structures where smaller model (here rows with removed variable group 1-5 in Table S4-Table S6) is compared to a model with larger number of predictors also including those in the smaller model (here model marked as “none” in Table S4-Table S6). Both data and the number of available data rows for the temperature classes differ, and therefore, comparison of the relative contribution between the temperature classes should be done with caution. Larger differences can be interpreted as a qualitative indication (e.g. local meteorology, group 3, has stronger influence in the organic mass during warmer months than during colder months, see Table S4). Smaller differences, however, can be easily overinterpreted (see e.g. relative contributions for both temperature classes for group 4b in Table S4) and conclusions should not be drawn based those values only.

**Table S4 Org as a response variable. Relative contribution as a difference in BIC as a percentage compared to full model (with all variable groups) when one group at a time is removed from the model. Correlation coefficient describes how well the changes in the observed data are captured by the model.**

Removed variable group	Relative contribution (%)		Correlation coef.	
	warm	cold	warm	cold
none	NA	NA	0.81	0.77
1	6.03	2.36	0.76	0.74
2	4.79	10.40	0.77	0.66
3	10.62	1.76	0.71	0.75
4	0.60	2.26	0.80	0.75
4a	0.45	2.21	0.81	0.75
4b	0.22	0.11	0.81	0.76
5	2.13	1.20	0.79	0.75

**Table S5 SO<sub>4</sub> as a response variable. Relative contribution as a difference in BIC as a percentage compared to full model (with all variable groups) when one group at a time is removed from the model. Correlation coefficient describes how well the changes in the observed data are captured by the model.**

Removed variable group	Difference (%)		Correlation coef.	
	warm	cold	warm	cold
none	NA	NA	0.64	0.73
1	15.13	9.68	0.55	0.68
2	17.93	18.04	0.54	0.64
3	0.01	0.05	0.64	0.73
4	0.13	0.89	0.64	0.72
4a	0.09	0.65	0.64	0.73
4b	0.01	0.10	0.64	0.73
5	4.00	9.33	0.62	0.69

**Table S6 eBC as a response variable. Relative contribution as a difference in BIC as a percentage compared to full model (with all variable groups) when one group at a time is removed from the model. Correlation coefficient describes how well the changes in the observed data are captured by the model.**

Removed variable group	Difference (%)		Correlation coef.	
	warm	cold	warm	cold
none	NA	NA	0.74	0.79
1	6.08	27.04	0.70	0.74
2	15.95	78.68	0.64	0.63
3	5.80	10.21	0.71	0.77
4	0.62	3.54	0.74	0.78
4a	0.62	3.28	0.74	0.78
4b	0.05	0.77	0.74	0.79
5	1.44	14.10	0.73	0.76

**Table S7 Regression coefficients and their standard errors from the full mixed effects model for Org. Model fixed intercepts ( $\beta_0$ ) were -5.45/-4.42 (warm/cold,  $\mu\text{g m}^{-3}$ ) and the standard deviations for random intercepts were 0.447/0.129 for hour, 0.631/0.493 for month, 0.565/0.243 for year and 0.284/0.048 for air mass source area for warm and cold months, respectively.**

Model predictor variable	Regression coefficient				Unit
	warm		cold		
	Slope ( $\beta_n$ )	Std. Error	Slope ( $\beta_n$ )	Std. Error	
NO <sub>x</sub>	6.25E-01	3.83E-01	2.64E-01	5.62E-03	$\mu\text{g m}^{-3}/\text{ppb}$
SO <sub>2</sub>	1.82E-01	2.92E-02	5.34E-01	5.29E-03	$\mu\text{g m}^{-3}/\text{ppb}$
O <sub>3</sub>	-1.68E-02	2.82E-02	3.43E-02	5.60E-03	$\mu\text{g m}^{-3}/\text{ppb}$
CO	3.22E-02	1.87E-03	2.48E-02	1.75E-03	$\mu\text{g m}^{-3}/\text{ppb}$

T	2.57E-01	8.15E-04	4.80E-02	5.17E-04	$\mu\text{g m}^{-3}/^{\circ}\text{C}$
MLH	-7.22E-01	3.44E-03	-6.85E-01	2.78E-03	$\mu\text{g m}^{-3}/\text{km}$
accum.precip*	-3.07E-02	3.26E-03	-6.47E-01	5.62E-03	$\text{mm}^{-1}$
time.in.cloud	-1.42E-02	1.31E-03	-6.25E-03	9.82E-04	$\mu\text{g m}^{-3}/\text{h}$
emission.col.time	-1.49E-04	5.65E-04	6.10E-03	5.57E-04	$\mu\text{g m}^{-3}/\text{h}$
time.in.land	8.62E-03	6.42E-04	7.25E-03	6.57E-04	$\mu\text{g m}^{-3}/\text{h}$

\* Note that this coefficient is in the exponent, see Eq. (2) from the main text.

**Table S8 Regression coefficients and their standard errors from the full mixed effects model for SO<sub>4</sub>. Model fixed intercepts ( $\beta_0$ ) were -1.79/-2.36 (warm/cold,  $\mu\text{g m}^{-3}$ ) and the standard deviations for random intercepts were 0.020/9.44E-11 for hour, 0.140/0.218 for month, 0.138/0.200 for year and 0.114/0.080 for airmass source area for warm and cold months, respectively.**

Model predictor variable	Regression coefficient				Unit
	warm		cold		
	Slope ( $\beta_n$ )	Std. Error	Slope ( $\beta_n$ )	Std. Error	
NOx	1.07E-01	9.75E-02	7.03E-03	1.29E-01	$\mu\text{g m}^{-3}/\text{ppb}$
SO <sub>2</sub>	3.01E-01	9.07E-03	7.62E-01	6.94E-03	$\mu\text{g m}^{-3}/\text{ppb}$
O <sub>3</sub>	1.53E-02	8.82E-03	1.01E-02	2.56E-02	$\mu\text{g m}^{-3}/\text{ppb}$
CO	5.90E-03	5.83E-04	7.40E-03	9.87E-04	$\mu\text{g m}^{-3}/\text{ppb}$
T	4.34E-03	2.54E-04	7.24E-03	2.67E-04	$\mu\text{g m}^{-3}/^{\circ}\text{C}$
MLH	-1.91E-02	1.05E-03	-1.94E-02	1.50E-03	$\mu\text{g m}^{-3}/\text{km}$
accum.precip*	-1.90E-03	4.24E-04	-7.96E-03	1.04E-03	$\text{mm}^{-1}$
time.in.cloud	1.37E-03	4.08E-04	2.00E-03	4.58E-04	$\mu\text{g m}^{-3}/\text{h}$
emission.col.time	7.38E-04	1.72E-04	2.49E-03	2.62E-04	$\mu\text{g m}^{-3}/\text{h}$
time.in.land	-9.09E-04	2.01E-04	6.00E-03	3.13E-04	$\mu\text{g m}^{-3}/\text{h}$

\* Note that this coefficient is in the exponent, see Eq. (2) from the main text.

**Table S9 Regression coefficients and their standard errors from the full mixed effects model for eBC. Model fixed intercepts ( $\beta_0$ ) were -1.38/-1.96 (warm/cold,  $\mu\text{g m}^{-3}$ ) and the standard deviations for random intercepts were 0.016/0.005 for hour, 0.024/0.116 for month, 0.049/0.078 for year and 0.015/0.010 for airmass source area for warm and cold months, respectively.**

Model predictor variable	Regression coefficient				Unit
	warm		cold		
	Slope ( $\beta_n$ )	Std. Error	Slope ( $\beta_n$ )	Std. Error	
NOx	9.08E-02	4.25E-03	4.79E-02	6.52E-03	$\mu\text{g m}^{-3}/\text{ppb}$
SO <sub>2</sub>	1.66E-02	2.13E-03	1.10E-01	2.57E-03	$\mu\text{g m}^{-3}/\text{ppb}$
O <sub>3</sub>	1.52E-03	2.09E-03	7.21E-03	5.54E-03	$\mu\text{g m}^{-3}/\text{ppb}$
CO	3.07E-03	1.55E-04	5.94E-03	3.66E-04	$\mu\text{g m}^{-3}/\text{ppb}$
T	9.38E-03	6.44E-05	8.81E-03	1.01E-04	$\mu\text{g m}^{-3}/^{\circ}\text{C}$

MLH	-5.51E-02	2.87E-04	-1.28E-01	5.75E-04	$\mu\text{g m}^{-3}/\text{km}$
accum.precip*	-1.38E-03	1.12E-04	-4.33E-03	3.58E-04	$\text{mm}^{-1}$
time.in.cloud	-5.05E-04	1.10E-04	-1.25E-03	1.83E-04	$\mu\text{g m}^{-3}/\text{h}$
emission.col.time	2.38E-04	4.65E-05	2.52E-03	1.05E-04	$\mu\text{g m}^{-3}/\text{h}$
time.in.land	3.28E-04	5.40E-05	1.24E-03	1.20E-04	$\mu\text{g m}^{-3}/\text{h}$

\* Note that this coefficient is in the exponent, see Eq. (2) from the main text.

#### 4 Source contribution and vertical transport of the airmasses

Source contribution analysis was applied to further confirm that e.g. the seasonal patterns of trace gases like SO<sub>2</sub> and aerosols shown in Riuttanen et al. (2013) also hold for our study period. For each back trajectory arrival time, a temporally collocated measurement made at the SMEAR II station is assigned to all grid cells visited by the corresponding trajectory. Grid cells visited by fewer than 10 trajectories are discarded. The median of values for each grid cell is then calculated to produce a concentration field. Finally, the percentage difference from the total median is calculated. This approach is similar to Riuttanen et al. (2013) however does not apply a weighting according to travelled distance.

To investigate the vertical transport, and exclude possible influence caused by e.g., low level transport of sulfate from the oceans into our results (which could show up as high sulfate concentrations when the airmass has spent more time under high humidity conditions), we looked into the airmass height provided by the HYSPLIT airmass trajectories. For this, the airmass height data along the trajectories was clustered with kmeans-clustering using the Hartigan-Wong algorithm (Hartigan and Wong, 1979) and 3 clusters were selected for further analysis. Additional clusters did not show new patterns, but only divided the cluster 3 into sub-clusters with different maximum heights. Figure S17 shows the median airmass height above ground along the trajectory with 25<sup>th</sup>-75<sup>th</sup> percentiles. Cluster 1 shows now the near-surface trajectories which could be transporting SO<sub>4</sub> from oceans along with high RH values, if the airmasses pass near sea surface. This cluster, however, has largest contribution of SO<sub>4</sub> from the continental Europe (Figure S18), indicating these airmasses are mostly affected by anthropogenic emissions of SO<sub>2</sub>, as sulfur from anthropogenic sources is mainly emitted as SO<sub>2</sub> (e.g. Paulot et al., 2017).

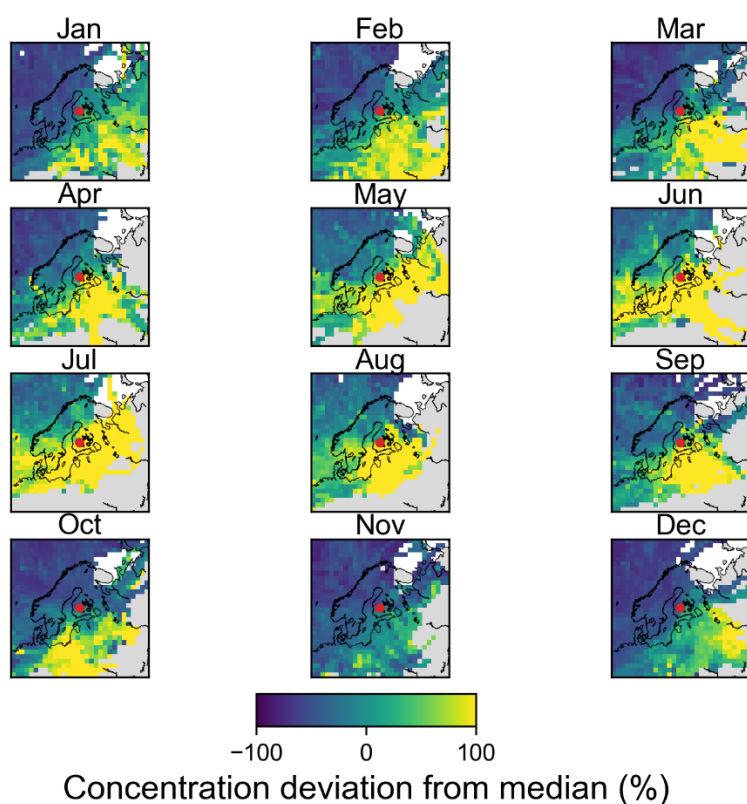


**Figure S15** Potential source contribution of accumulation mode ( $dp = 100 \text{ nm} - 1000 \text{ nm}$ ) particle number concentration in SMEAR II. Concentration fields are normalized to the median concentration over the whole measurement data. Data is shown for years between 2012-2019 which overlaps with the composition measurements. Pre-processed data is shown, thus trajectories crossing Kola Peninsula and trajectories arriving to SMEAR II with wind direction between 120°-140° are not included. Red dot shows the location of SMEAR II.

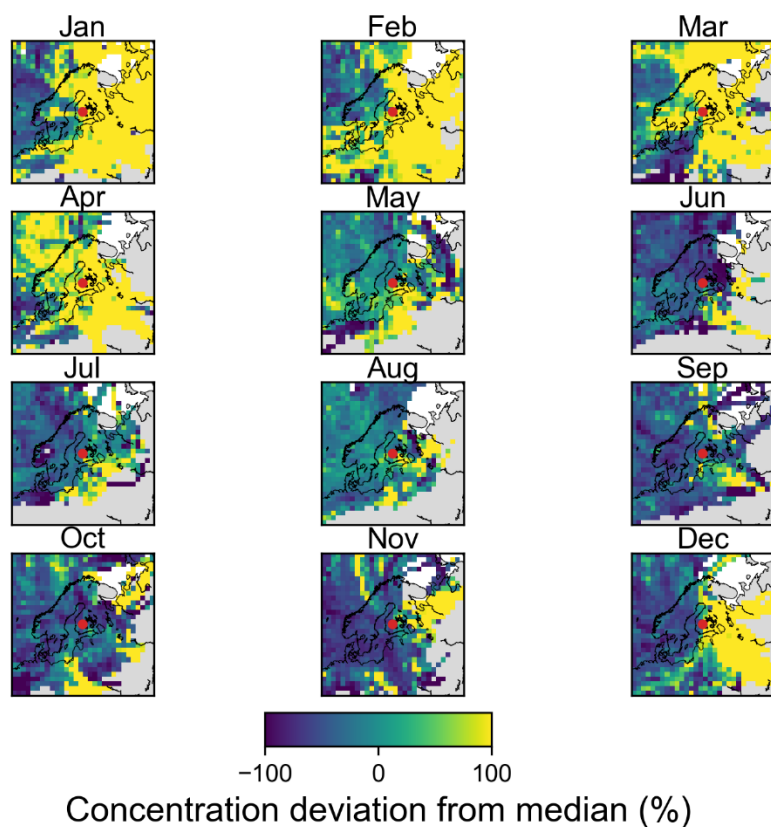


Figure S16 Potential source contribution of SO<sub>2</sub> concentration in SMEAR II. Concentration fields are normalized to the median concentration over the whole measurement data. Data is shown for years between 2012-2019 which overlaps with the composition measurements. Pre-processed data is shown, thus trajectories crossing Kola Peninsula and trajectories arriving to SMEAR II with wind direction between 120°-140° are not included. Red dot shows the location of SMEAR II.

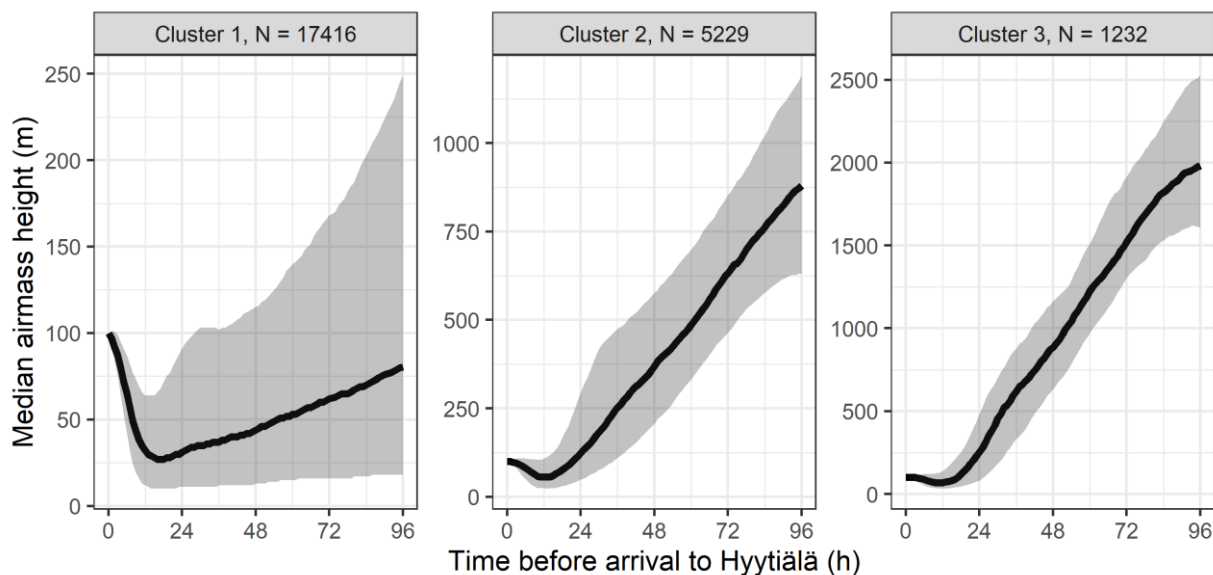


Figure S17 Median airmass height for each cluster (black lines) with 25<sup>th</sup>-75<sup>th</sup> percentiles (shaded area). The figure includes collocated observations of the trajectory data and measured SO<sub>4</sub>/Org/BC, thus including time between March 2012 and August 2019. N shows the number of data rows in each cluster.

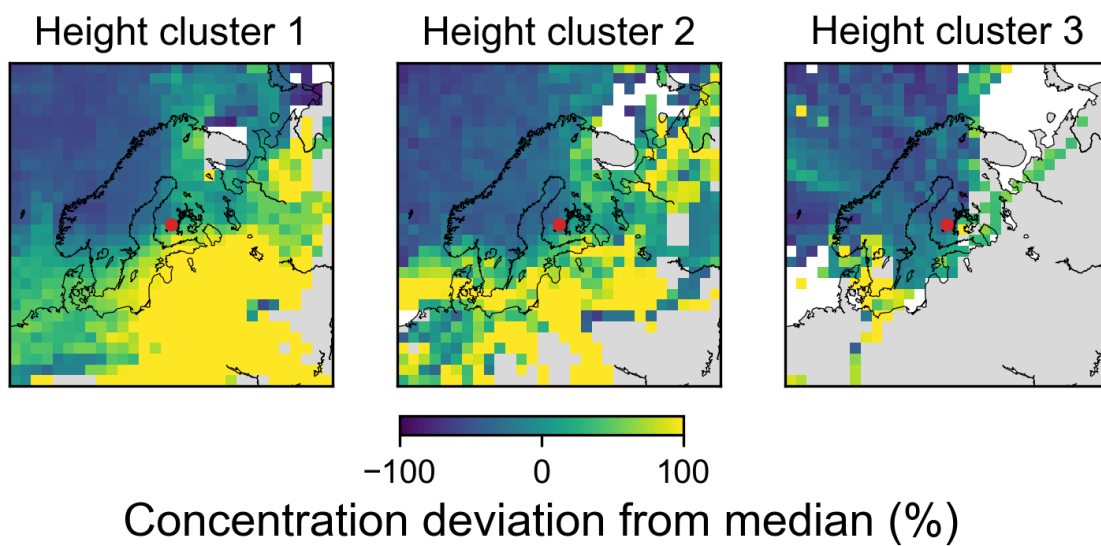


Figure S18 Potential source contribution of SO<sub>4</sub> for each height cluster shown in Figure S17. Red dot shows the location of SMEAR II.



## 5 Main figures with HYSPLIT trajectories using GDAS reanalysis meteorology

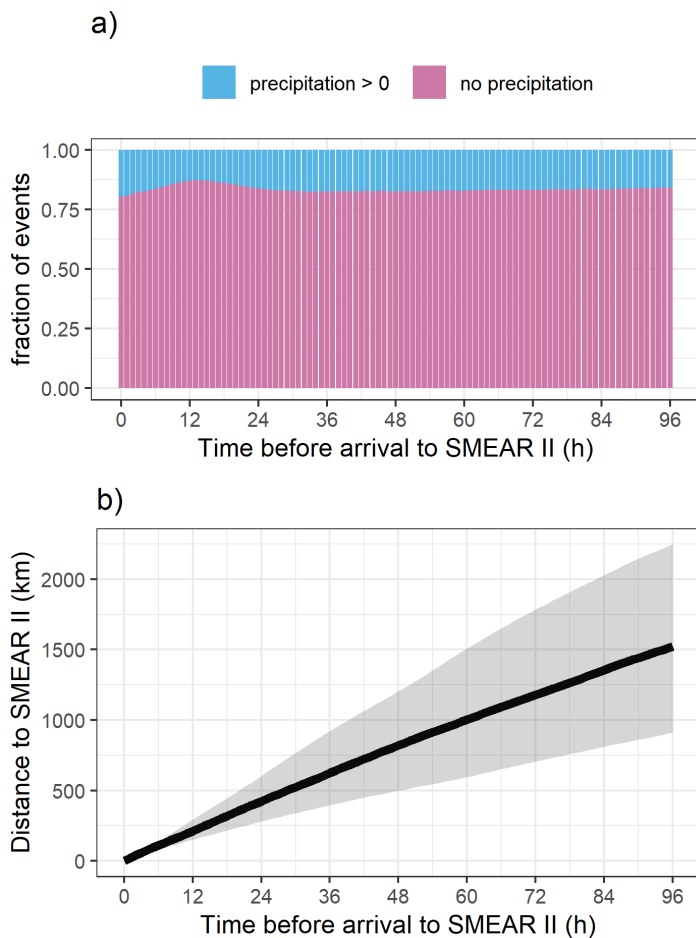


Figure S19 Fraction of precipitation events (based on GDAS meteorology) along the trajectory is shown in a) and b) shows the median distance from SMEAR II with shaded area showing the 25<sup>th</sup>-75<sup>th</sup> percentiles.

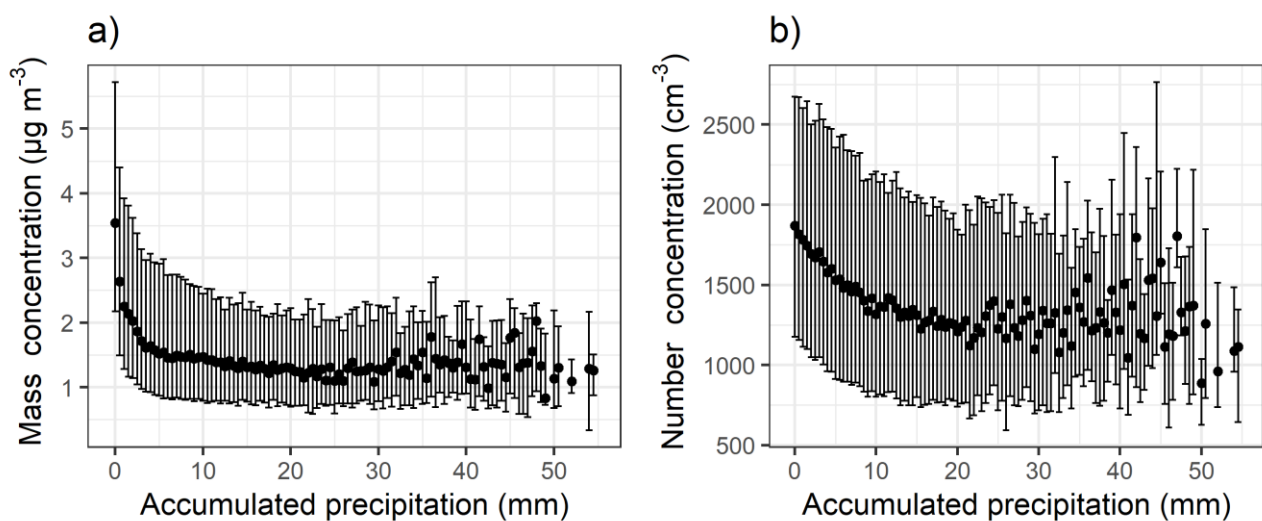


Figure S20 Total particle ( $d_p = 3\text{-}1000\text{ nm}$ ) mass (a) and number (b) concentration as a function of 0-50 mm accumulated precipitation along the 96-hour HYSPLIT air mass trajectories based on GDAS meteorology. The black dots show the median values and bars highlight the 25<sup>th</sup>-75<sup>th</sup> percentiles for each 0.5 mm bin of accumulated precipitation. The figure includes DMPS data between January 2005 and August 2019.

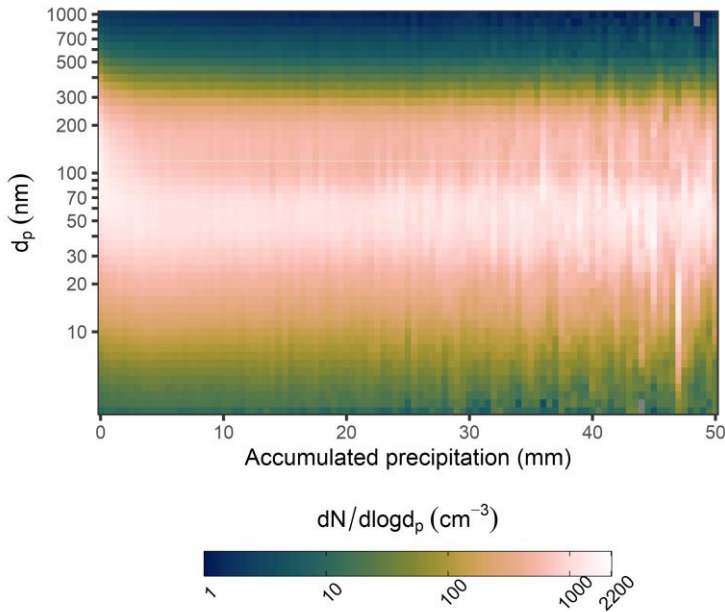


Figure S21 The aerosol size distribution ( $d_p = 3\text{-}1000$  nm) as a function of the 0-50 mm of accumulated precipitation along the 96-hour air mass trajectories based on GDAS meteorology. Data is shown as medians for binned accumulated precipitation (bin size 0.5 mm). Grey areas show missing data and/or values where  $dN/d\log d_p < 1$ . The figure includes DMPS data between January 2005 and August 2019.

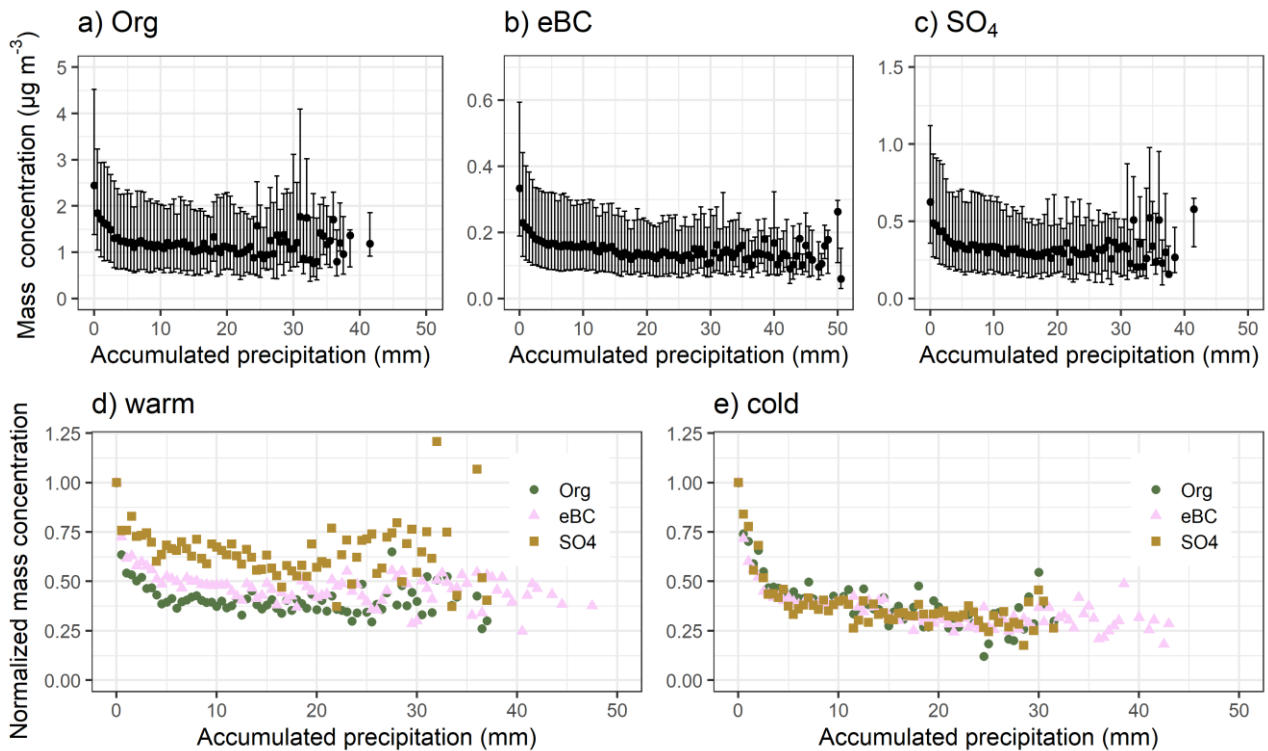


Figure S22 Particle mass concentration of a) Org, b) eBC and c) SO<sub>4</sub> as a function of accumulated precipitation along the 96-hour air mass trajectories based on GDAS meteorology. The black dots in the top row show the median values and bars highlight the 25<sup>th</sup>-75<sup>th</sup> percentiles for each 0.5 mm bin of accumulated precipitation. Bottom row shows normalized particle masses (calculated from the medians) with temperature separation. Medians and normalized medians are shown for each bin having 10 or more data points. The figure includes data between 2006-2019 for eBC and 2012-2019 for Org and SO<sub>4</sub>.

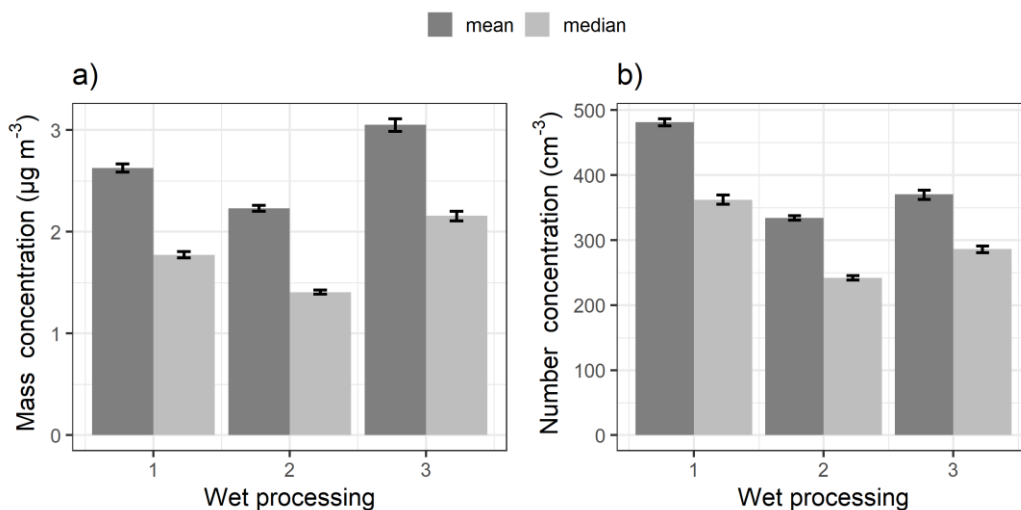


Figure S23 Median and mean accumulation mode ( $d_p = 100\text{-}1000\text{ nm}$ ) particle mass (a) and number (b) concentration for wet processing groups (trajectories based on GDAS meteorology) described in Table . The figure includes DMPS data between January 2005 and August 2019. The whiskers show the 99 % confidence intervals from 1000 bootstrap replicates.

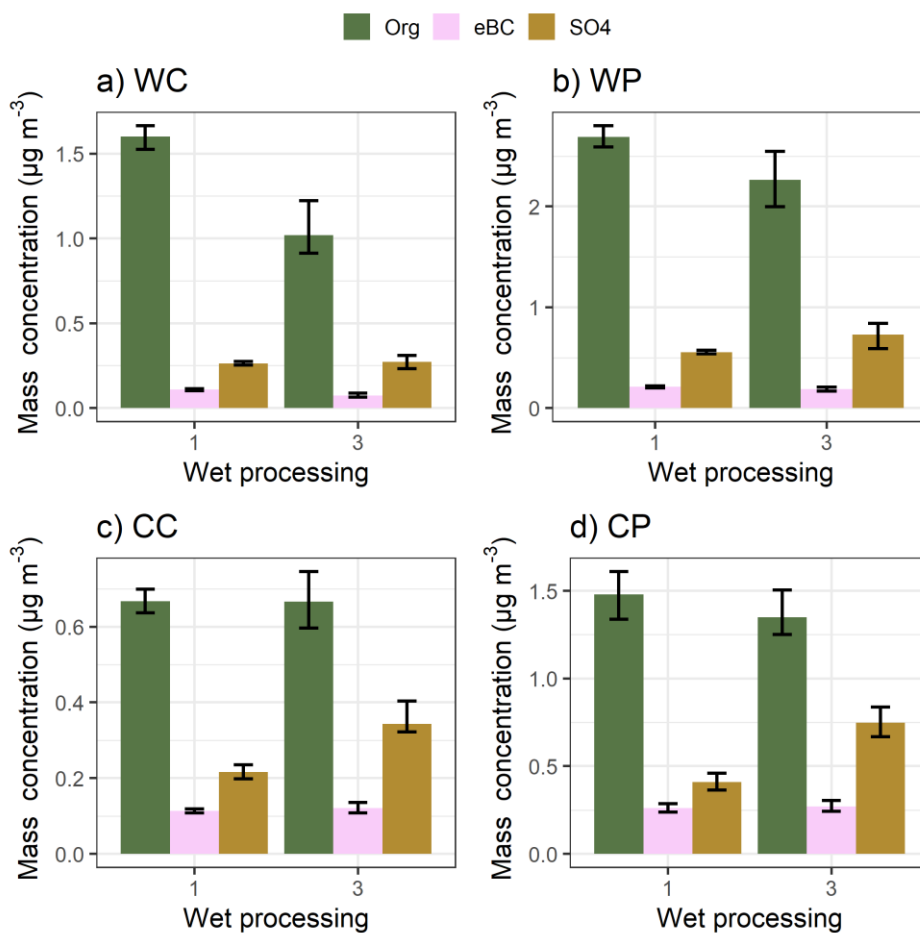


Figure S24 Median particle mass concentration for Org, eBC and  $\text{SO}_4$  for wet processing groups (trajectories based on GDAS meteorology) 1 and 3 as described in in Table 2 in the main text. Subplots show the air mass sectors (clean and polluted) with the seasonal (warm and cold) division followingly: a) warm and clean, b) warm and polluted, c) cold and clean and b) cold and polluted. The figure is based on simultaneous observations of these three species between March 2012 and August 2019. The whiskers show the 99 % confidence intervals from 1000 bootstrap replicates. Note the different y-axis limits in each subplot.

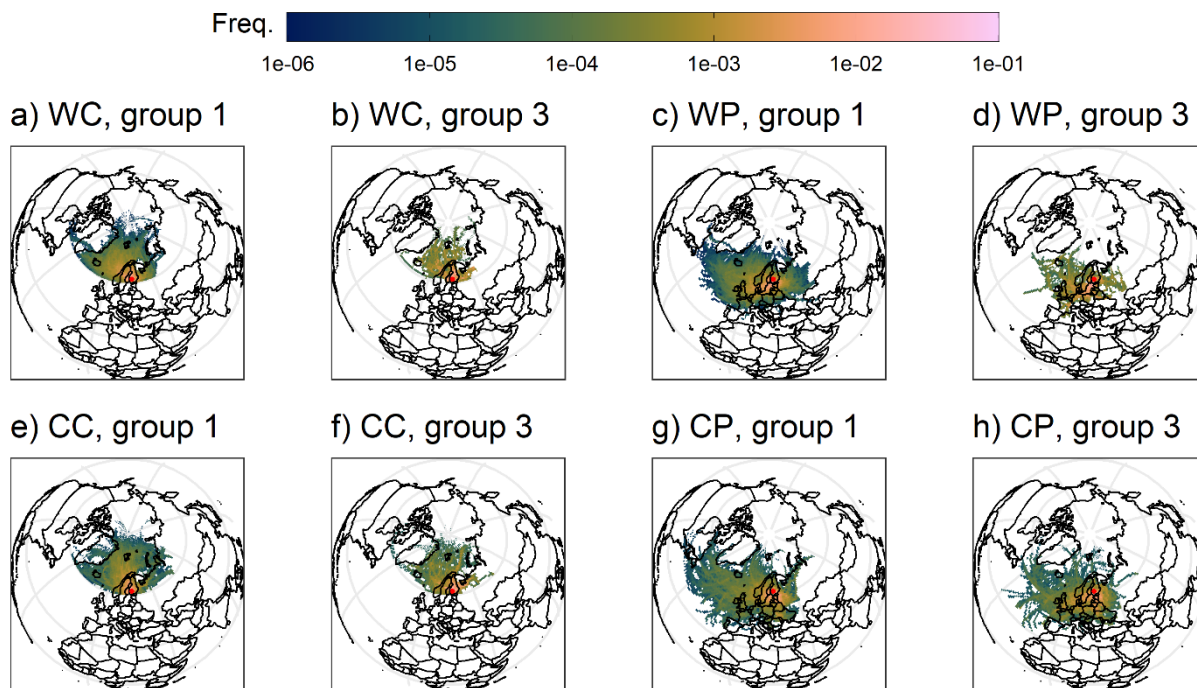


Figure S25 96-hour air mass history (trajectories based on GDAS meteorology) for the wet processing groups with the sector (clean and polluted) and temperature (warm and cold) division. Subplots show a)-b) warm and clean, c)-d) warm and polluted, e)-f) cold and clean and g)-h) cold and polluted. Colour scale shows the frequency (crossings in each  $1^\circ \times 1^\circ$  grid point divided by total number of crossings in each group) of trajectories crossing a grid point. The groups 1 and 3 correspond to the air mass history groups presented in Table 2 in the main text. The red dot shows the location for SMEAR II.

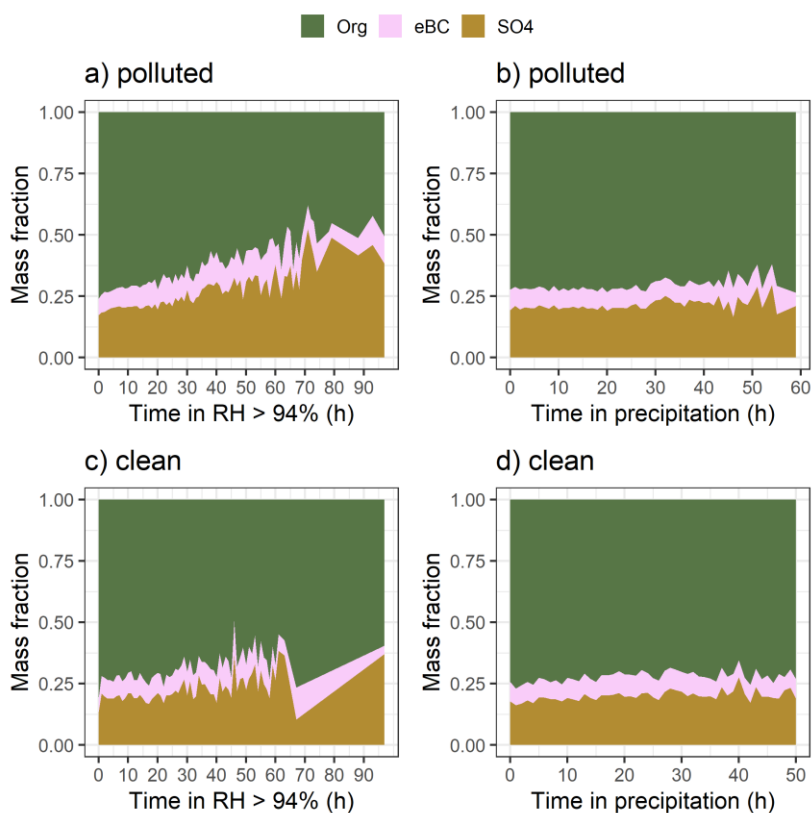
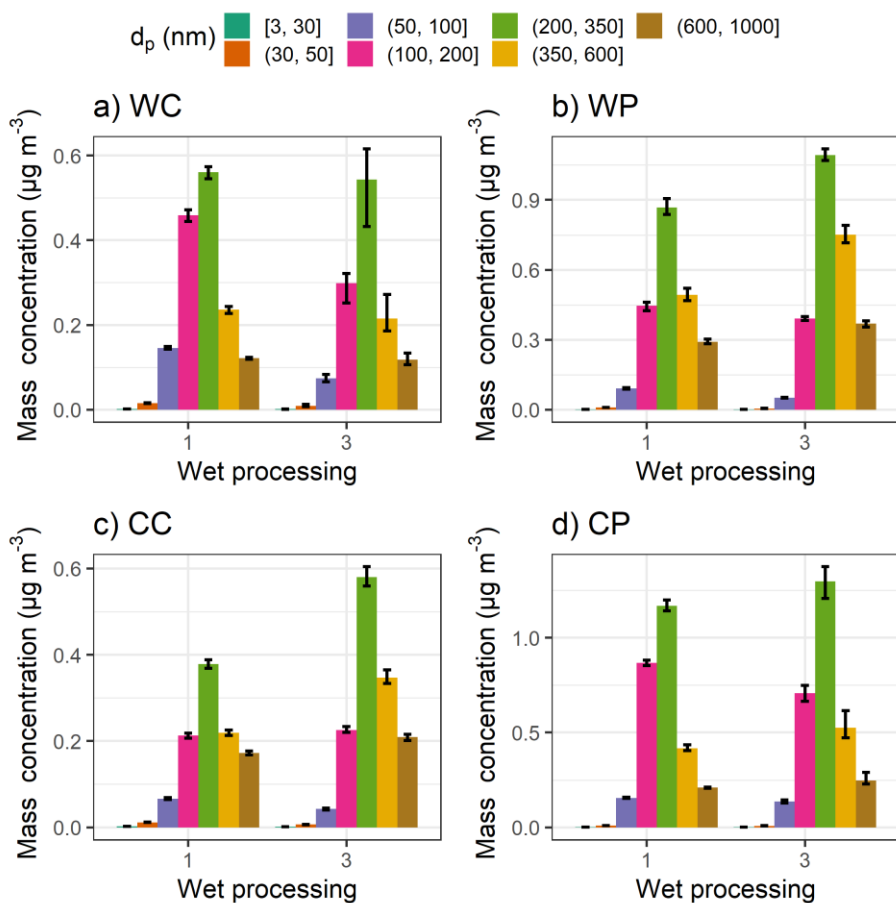


Figure S26 The mass fractions of Org, SO<sub>4</sub> and eBC for clean and more polluted air masses as a function of time spent in RH > 94 % (a and c) and in precipitation (b and d): Figure shows median values for each 1-hour bin, if 10 or more data points were available in the bin. The figure is based on observations between March 2012 and August 2019. Trajectories based on GDAS meteorology.



**Figure S27** Median particle mass concentration for size bins derived from the DMPS measurements for wet processing groups 1 and 3 as described in Table 2 in the main text. Subplots show the air mass sectors (clean and polluted) with the seasonal (warm and cold) division followingly: a) warm and clean, b) warm and polluted, c) cold and clean and b) cold and polluted. The figure includes all available data between January 2005 and August 2019. The whiskers show the 99 % confidence intervals from 1000 bootstrap replicates. Note the different y-axis scale in each subplot. Trajectory data based on GDAS meteorology.

## References

- Hartigan, J. A., and Wong, M. A.: Algorithm AS 136: A K-Means Clustering Algorithm, *Journal of the Royal Statistical Society. Series C (Applied Statistics)*, 28, 100-108, 10.2307/2346830, 1979.
- Paulot, F., Fan, S., and Horowitz, L. W.: Contrasting seasonal responses of sulfate aerosols to declining SO<sub>2</sub> emissions in the Eastern U.S.: Implications for the efficacy of SO<sub>2</sub> emission controls, *Geophysical Research Letters*, 44, 455-464, <https://doi.org/10.1002/2016GL070695>, 2017.
- Riuttanen, L., Hulkkonen, M., Dal Maso, M., Junninen, H., and Kulmala, M.: Trajectory analysis of atmospheric transport of fine particles, SO<sub>2</sub>, NO<sub>x</sub> and O<sub>3</sub> to the SMEAR II station in Finland in 1996&ndash;2008, *Atmos. Chem. Phys.*, 13, 2153-2164, 10.5194/acp-13-2153-2013, 2013.
- Schwarz, G.: Estimating the Dimension of a Model, *The Annals of Statistics*, 6, 461-464, 464, 1978.
- Stoica, P., and Selen, Y.: Model-order selection: a review of information criterion rules, *IEEE Signal Processing Magazine*, 21, 36-47, 10.1109/msp.2004.1311138, 2004.
- Virkkula, A., Mäkelä, T., Hillamo, R., Yli-Tuomi, T., Hirsikko, A., Hämeri, K., and Koponen, I. K.: A Simple Procedure for Correcting Loading Effects of Aethalometer Data, *Journal of the Air & Waste Management Association*, 57, 1214-1222, 10.3155/1047-3289.57.10.1214, 2007.